

# Nickel Complexes Based on Thiophenedithiolate Ligands – Magnetic Properties of Metallocenium Salts

Dulce Belo,<sup>[a]</sup> Helena Alves,<sup>[a]</sup> Sandra Rabaça,<sup>[a]</sup> Laura Cristina Pereira,<sup>[a]</sup>  
Maria Teresa Duarte,<sup>[b]</sup> Vasco Gama,<sup>[a]</sup> Rui Teives Henriques,<sup>[a]</sup> Manuel Almeida,<sup>\*,[a]</sup>  
Elisabet Ribera,<sup>[c]</sup> Concepció Rovira,<sup>[c]</sup> and Jaume Veciana<sup>[c]</sup>

**Keywords:** S ligands / Coordination chemistry / Magnetic properties / Nickel

The nickel complex  $n\text{Bu}_4\text{N}[\text{Ni}(\alpha\text{-tpdt})_2]$  (**2**) ( $\alpha\text{-tpdt}$  = 2,3-thiophenedithiolate) has been prepared and characterized. A salt of this monoanionic paramagnetic complex,  $[\text{Fe}(\text{Cp}^*)_2][\text{Ni}(\alpha\text{-tpdt})_2]$  (**3**), was obtained with decamethylferrocene, crystallizing in the monoclinic space group  $P2_1/a$  with  $a = 15.443(3)$ ,  $b = 10.237(1)$ ,  $c = 20.360(2)$  Å,  $\beta = 107.54(1)^\circ$ ,  $V = 3069.1(7)$  Å<sup>3</sup>,  $Z = 4$ . Its structure consists of alternating cationic and anionic layers, with short interlayer contacts defining alternating cation–anion chains. Magnetic characterization of **3** at low applied magnetic fields revealed an antiferro-

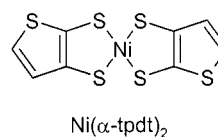
magnetic transition at  $T_N = 2.56$  K. Below  $T_N$ , **3** displays a metamagnetic behaviour with a critical field of 0.07 T at 1.6 K. The magnetic properties of this compound are compared with those of the analogous salts with diamagnetic gold dithiolate  $[\text{Fe}(\text{Cp}^*)_2][\text{Au}(\alpha\text{-tpdt})_2]$  (**4**), and diamagnetic decamethylcobaltocenium,  $[\text{Co}(\text{Cp}^*)_2][\text{Ni}(\alpha\text{-tpdt})_2]$  (**5**), which are also reported. This comparison shows that the ferromagnetic interactions observed in **3** are due to cation–anion intra-chain interactions.

## Introduction

Square-planar bis(dithiolene) transition metal complexes have attracted considerable interest, essentially in their use as building blocks for constructing molecular materials. They are versatile units that can have a wide range of oxidation states, coordination geometries, and magnetic moments.<sup>[1]</sup> To date they have been used to generate several interesting and unusual properties, such as metallic behaviour<sup>[2]</sup> or even superconductivity,<sup>[3,4]</sup> third-order nonlinear optical properties, and cooperative magnetic properties such as ferromagnetism<sup>[5]</sup> or metamagnetism.<sup>[6]</sup>

In a recent paper, we reported the preparation of gold complexes based on three different thiophenedithiolate ligands.<sup>[7]</sup> They were viewed as the first members of a new larger family of complexes with different transition metals. These complexes have a high potential for use as building blocks in the preparation of novel molecular materials with interesting conducting or magnetic properties.

In this paper, we report the synthesis and characterization of the first nickel complex belonging to this series in the form of a tetrabutylammonium salt,  $n\text{Bu}_4\text{N}[\text{Ni}$



Scheme 1

$(\alpha\text{-tpdt})_2]$ , where  $\alpha\text{-tpdt}$  = 2,3-thiophenedithiolate (Scheme 1). The synthesis, crystal structure, and magnetic properties of the decamethylferrocenium charge-transfer (CT) salt are also reported and are compared with those of the analogous salts with the diamagnetic acceptor (A)  $[\text{Fe}(\text{Cp}^*)_2][\text{Au}(\alpha\text{-tpdt})_2]$  and the diamagnetic donor (D)  $[\text{Co}(\text{Cp}^*)_2][\text{Ni}(\alpha\text{-tpdt})_2]$ .

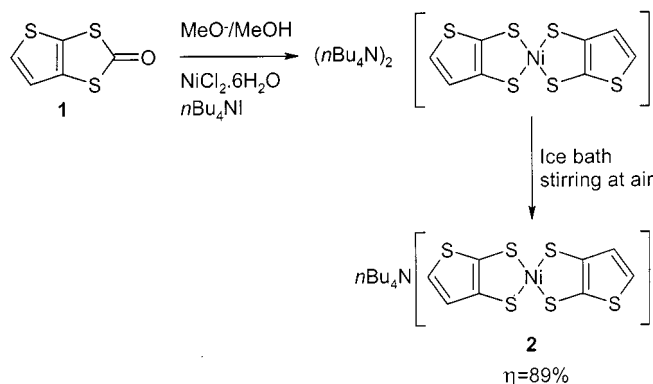
## Results and Discussion

The synthesis of  $n\text{Bu}_4\text{N}[\text{Ni}(\alpha\text{-tpdt})_2]$  was carried out following a procedure (Scheme 2) similar to that described previously for the gold analogue.<sup>[7]</sup> The thiophenedithiolate ligands were obtained from 5,6-thieno[2,3-*d*]-1,3-dithiol-2-one (**1**) in methanol solution by cleavage with potassium methoxide. The ligand solution thus obtained, without isolation of the intermediate, was immediately added to a solution of nickel dichloride in methanol to give the nickel species, which precipitated as the green tetrabutylammonium salt  $n\text{Bu}_4\text{N}[\text{Ni}(\alpha\text{-tpdt})_2]$  (**2**) upon treatment with  $n\text{Bu}_4\text{NI}$  followed by stirring in air at ice-bath temperature. The precipitate was washed with methanol and purified by recrystallization from acetone/2-propanol to give air-stable crystals. The final yield was 89%. Elemental analysis results

<sup>[a]</sup> Instituto Tecnológico e Nuclear, Estrada nacional no. 10, 2686–953 Sacavém, Portugal  
Fax: (internat.) + 351-21/994-1455  
E-mail: malmeida@itn1.itn.pt

<sup>[b]</sup> Instituto Superior Técnico, Av. Rovisco Pais, 1049–001 Lisboa, Portugal  
Fax: (internat.) + 351-21/841-7862  
E-mail: teresa.duarte@ist.utl.pt

<sup>[c]</sup> Institut de Ciència de Materials de Barcelona (CSIC), Campus Universitari de Bellaterra, 08193 Cerdanyola, Spain  
Fax: (internat.) + 34-93/5805729  
E-mail: cun@icmab.es



Scheme 2

correspond to a 1:1 stoichiometry for the  $n\text{Bu}_4\text{N}$  salts of the nickel complex, thus indicating that  $\text{Ni}^{\text{II}}$  is oxidized during the synthesis.

Cyclic voltammetry of **2** in acetonitrile shows a pair of symmetric reversible redox waves at  $E_{1/2} = -0.562$  V vs.  $\text{Ag}/\text{AgCl}$ , corresponding to the couple  $[\text{Ni}(\alpha\text{-tpdt})_2]^{2-}/[\text{Ni}(\alpha\text{-tpdt})_2]^-$ . At higher potentials, a pair of reversible waves is seen at  $E_{1/2} = 0.253$  V, corresponding to the couple  $[\text{Ni}(\alpha\text{-tpdt})_2]^-/[\text{Ni}(\alpha\text{-tpdt})_2]$ . Similar voltammograms and almost identical potentials are observed in dichloromethane solution.

Oxidation potentials indicate that it is easier to obtain the neutral species in the case of the nickel complex than for the gold analogue, for which the couples  $\text{Au}^{\text{II}}/\text{Au}^{\text{III}}$  and  $\text{Au}^{\text{III}}/\text{Au}^{\text{IV}}$  were found under the same conditions at  $-1.62$  V and  $0.456$  V, respectively.<sup>[7]</sup> In fact, solutions of compound **2** are rather unstable in air and decompose to give a fine precipitate, faster than in the case of the Au analogue.

In spite of the fact that well-formed single crystals are easily obtained, the crystal structure of **2**, with cell parameters  $a = 9.4801(19)$ ,  $b = 18.7867(24)$ ,  $c = 9.6185(20)$  Å,  $\beta = 119.336(23)^\circ$ ,  $V = 1493(1)$  Å<sup>3</sup>, could not be solved due to severe twinning problems.

$\text{Ni}^{\text{III}}$ , having a  $d^7$ -electronic configuration, in the square-planar coordination anticipated for  $[\text{Ni}(\alpha\text{-tpdt})_2]^-$ , is expected to be paramagnetic with  $S = 1/2$ . This was confirmed by EPR and magnetization measurements.

The powder EPR spectrum of salt **2** at 7.5 K is shown in Figure 1, a. The spectrum observed in frozen acetone solutions, as shown in Figure 1, b, gives similar  $g$  values, with a structure corresponding to a rhombic anisotropy with

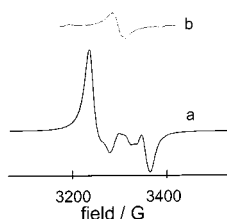


Figure 1. EPR spectra of compound **2**: (a) powder at 7.5 K, (b) acetone solution at 60 K

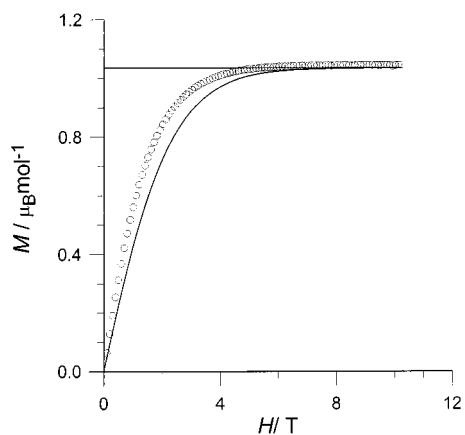


Figure 2. Magnetization of compound **2** as a function of the field at 1.6 K

values of  $g_1 = 2.11492$ ,  $g_2 = 2.04992$ ,  $g_3 = 1.99611$ . Single-crystal data show a single line of width 20 G at 8 K.

The static paramagnetic susceptibility of compound **2** follows the Curie–Weiss law with  $\theta = 2.1$  K and indicates an effective magnetic moment,  $\mu_{\text{eff}}$ , of  $1.76 \mu_{\text{B}}$ . The presence of slight ferromagnetic interactions in this compound, as denoted by the small positive  $\theta$  value, is confirmed by the magnetization field dependence at 1.6 K (Figure 2), which shows a saturation magnetization of  $1.04 N\mu_{\text{B}}$ . This is approached more rapidly than predicted by the Brillouin function for an  $S = 1/2$  spin system with an average  $\langle g \rangle = 2.06$  (thin solid curve). In most cases, the salts of metal-bis(dichalcogenide) monoanionic complexes with diamagnetic cations exhibit antiferromagnetic interactions, while in the case of compound **2** the coupling between the complexes is ferromagnetic. However, the absence of a crystal structure precludes a discussion of the contacts that give rise to the ferromagnetic interactions. In view of this, efforts towards the determination of the structure of compound **2** will be made.

The CT salt **3** and the corresponding analogues with decamethylcobaltocenium,  $[\text{Co}(\text{Cp}^*)_2][\text{Ni}(\alpha\text{-tpdt})_2]$  (**4**), and gold-bis(thiophenedithiolate),  $[\text{Fe}(\text{Cp}^*)_2][\text{Au}(\alpha\text{-tpdt})_2]$  (**5**), were obtained as small crystals by addition of equimolar solutions of a decamethylmetallocene salt and  $n\text{Bu}_4\text{N}-[\text{M}'(\alpha\text{-tpdt})_2]$ , respectively, under anaerobic conditions. Single crystals suitable for structural and physical studies were obtained by slow evaporation of the solvent from saturated acetonitrile solutions.

The crystal structure of compound **3** was solved. It crystallizes in the monoclinic space group  $P2_1/a$  with  $Z = 4$ . Crystal and experimental data are summarized in Table 2. The systematic absences confirm the space group as  $P2_1/a$ . In the asymmetric unit, we found two half- $[\text{Fe}(\text{Cp}^*)_2]^+$  fragments, the Fe atoms lying in special positions (centres of symmetry), and one acceptor molecule,  $[\text{Ni}(\alpha\text{-tpdt})_2]$ , the Ni atom residing far from any special position. A significant disorder was observed in the methyl groups of the  $\text{Cp}^*$  fragments; several disorder models were tried but none seemed to bring any improvement in the structure refine-

ment, not by lowering the e.s.d. in the bond lengths and angles nor by lowering the  $R$  values. Thus, the Me groups were allowed to refine anisotropically with an ISOR restraint of 0.02.

The Cp rings of the donor adopt a staggered conformation, as is commonly found. The  $[\text{Ni}(\alpha\text{-tpdt})_2]^-$  anion adopts only a *trans* ( $E$ ) configuration in the crystal, in analogy with the salt of a gold complex with the similar non-aromatic ligand dtpdt,  $n\text{Bu}_4\text{N}[\text{Au}(\text{dtpdt})_2]$ .<sup>[7]</sup> The Ni–S bond lengths observed in the Ni complex, with average values of 2.156 Å (see Table 1), are in a good agreement with the values reported for other  $\text{Ni}^{\text{III}}$  dithiolates.<sup>[8–10]</sup> The  $[\text{Ni}(\alpha\text{-tpdt})_2]^-$  anion is almost planar with a small chair-type distortion (Figure 3).

The crystal structure of **3** consists of alternating layers of donors,  $[\text{Fe}(\text{Cp}^*)_2]^+$ , and acceptors,  $[\text{Ni}(\alpha\text{-tpdt})_2]^-$ , extending parallel to the  $a,b$  plane. This is illustrated in Figure 4, which shows a projection of the crystal structure along the  $a$  axis. Unlike the donor layers, in which the cations are quite isolated from each other, in the acceptor layers relatively short interionic AA distances are found involving S atoms of the central  $\text{NiS}_4$  fragment and a C atom of the thiophenic fragment of the ligand, as shown in Figure 5. The  $\text{S}\cdots\text{C}$  separations are 3.723 and 3.751 Å, exceeding the sum of the van der Waals radii (3.450 Å) by 8 and 9%, respectively. Short interlayer interionic DA distances are also seen, involving C atoms of the Cp rings and the S atom of the thiophenic fragment from the acceptors, as shown in Figure 4 (dashed lines). These  $\text{S}\cdots\text{C}$  distances are 3.530 and 3.610 Å, exceeding the sum of the van der Waals radii by 2 and 5%, respectively. These contacts form another set of layers composed of parallel alternating DA chains, as shown in Figure 6, and the chains in adjacent layers are almost perpendicular to each other, extending along directions alternating from  $2b + c$  to  $2b - c$  (Figure 7).

Table 1. Selected bond lengths and angles for  $[\text{Fe}(\text{Cp}^*)_2][\text{Ni}(\alpha\text{-tpdt})_2]$  (**3**)

	$d$ (Å)
Ni–S(1)	2.154(3)
Ni–S(2)	2.162(4)
Ni–S(3)	2.150(3)
Ni–S(4)	2.160(4)
S(1)–C(1)	1.703(13)
S(2)–C(2)	1.745(11)
S(3)–C(3)	1.736(12)
S(4)–C(4)	1.716(12)
S(5)–C(6)	1.703(14)
S(5)–C(1)	1.725(11)
S(6)–C(8)	1.732(16)
S(6)–C(3)	1.719(12)
C(1)–C(2)	1.387(14)
C(2)–C(5)	1.455(14)
C(3)–C(4)	1.346(15)
C(4)–C(7)	1.492(15)
C(5)–C(6)	1.361(15)
C(7)–C(8)	1.341(18)

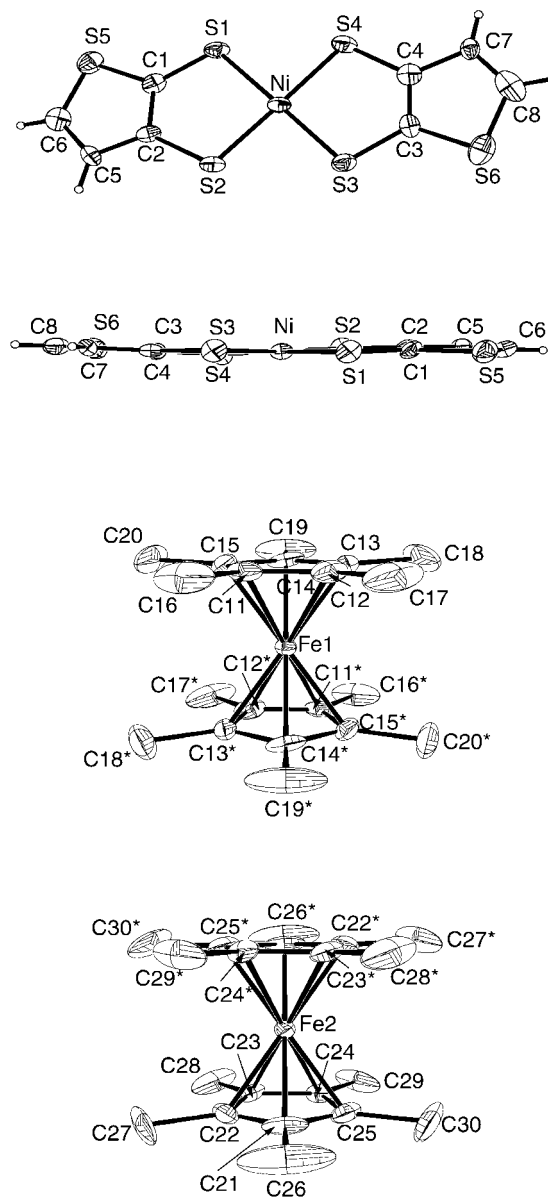


Figure 3. ORTEP diagram and atomic numbering scheme of compound **3** with thermal ellipsoids drawn at a 20% probability level; the high thermal vibration of the methyl groups is due to the disorder referred to in the text

The linear chain-based layers, extending parallel to the  $b,c$  plane ( $bc$  layers) are connected by the acceptor–acceptor interactions shown in Figure 5 forming a 3D network. Two chains from adjacent layers are shown in Figure 7 along with one anionic  $ac$  layer. The  $\text{S}\cdots\text{C}$  contacts are slightly shorter in the  $b,c$  layers than in the  $a,b$  layers. However, in this case it is not possible to predict which ones dominate the magnetic interactions, as this also depends on the spin densities of the atoms involved in the contacts.

In view of this crystal structure, if the  $ab$  intralayer (AA) and  $bc$  intralayer (DA) contacts are different in nature, a complex magnetic behaviour can be expected for compound **3**, where both the donor and acceptor units are paramag-

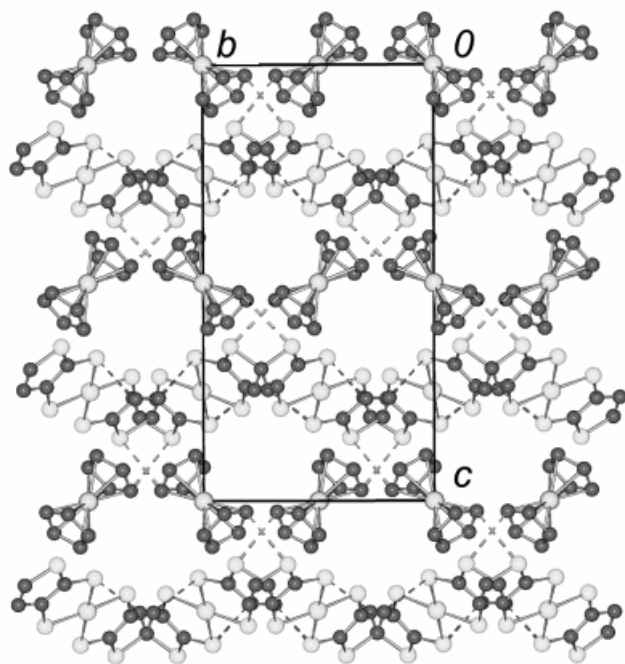


Figure 4. Crystal structure of **3** viewed along the *a* axis showing alternating layers of donors,  $[\text{Fe}(\text{Cp}^*)_2]^+$ , and acceptors,  $[\text{Ni}(\alpha\text{-tpdt})_2]^-$ , extending parallel to the *a,b* plane

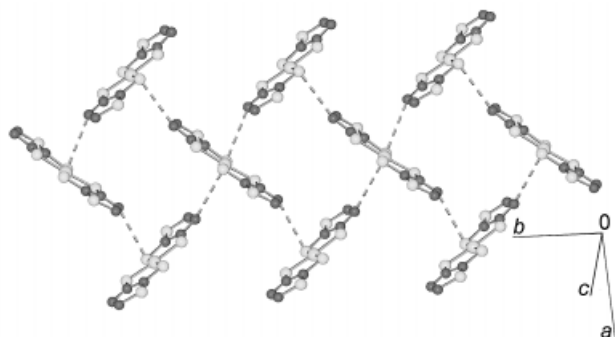


Figure 5. Layers of  $[\text{Ni}(\alpha\text{-tpdt})_2]^-$  in **3** showing the closest S...C contacts

netic species with localized  $S = 1/2$  spins. The nature of these interactions can be better understood through studying the magnetic properties of the two other analogous CT salts **4** and **5**, in which one of the species, either the donor, as  $[\text{Co}(\text{Cp}^*)_2]^+$ , or the acceptor, as  $[\text{Au}(\alpha\text{-tpdt})_2]^-$ , is diamagnetic.

For compound **4**, the crystal structure could not be refined due to lower quality of the crystals, but the X-ray diffraction data reveal a monoclinic unit cell with parameters of  $a = 15.370(3)$ ,  $b = 10.233(2)$ ,  $c = 20.450(3)$  Å,  $\beta = 108.41(3)^\circ$ , indicating that it is isostructural with **3**. In the case of **5**, it was not possible to determine the unit cell parameters.

The temperature dependence of the product of the static paramagnetic susceptibility  $\chi_P$  and the absolute temperature  $T$ ,  $\chi_P T$ , for compounds **3**, **4**, and **5** is shown in Figure 8. In the latter two cases,  $\chi_P T$  decreases upon cooling

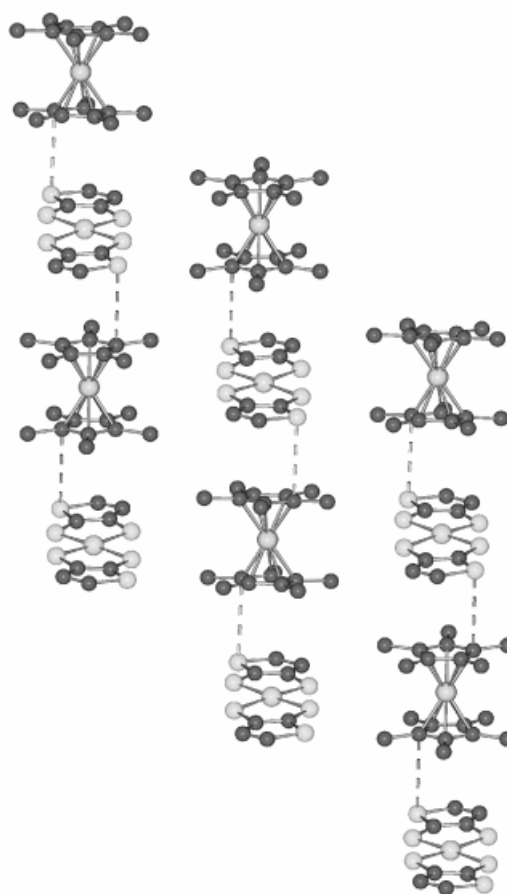


Figure 6. Partial view of the crystal structure of **3** showing the parallel alternating DA chains

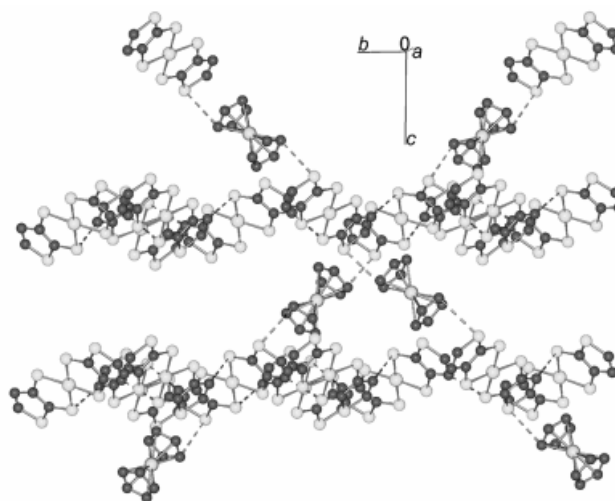


Figure 7. Partial view of the crystal structure of **3** illustrating the orthogonal DA chain directions

indicating that for the CT salt **4** the AA interactions are antiferromagnetic and that for compound **5** the DD interactions are antiferromagnetic. In the case of **3**, a broad minimum was observed at 130 K, and at lower temperatures a faster increase upon cooling was detected, indicating that

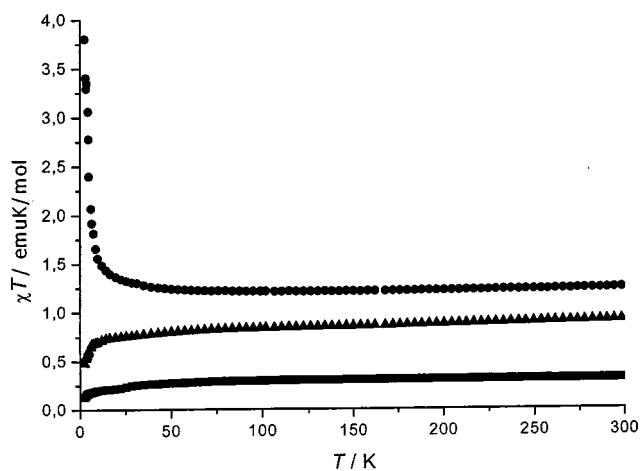


Figure 8. Temperature dependence of the product of the absolute temperature,  $T$ , with the static paramagnetic susceptibility,  $\chi_B$ , for salts **3** (circles), **4** (triangles), and **5** (squares)

under these conditions the dominant interactions are ferromagnetic.

At low temperatures, a field-dependent behaviour was observed in the magnetization temperature dependence of compound **3**, as shown in Figure 9. At low fields, e.g. at 15 mT, a maximum in the magnetization was observed at 2.5 K, indicating the existence of an antiferromagnetic transition. On increasing the applied magnetic field, the maximum shifts towards lower temperatures and at 30 mT it occurs at 2.35 K. At fields of greater than 70 mT the maximum is suppressed, suggesting a metamagnetic behaviour. The Néel temperature of the antiferromagnetic transition in this compound was determined by low-field (1 Oe) AC magnetic susceptibility measurements through the observation of a sharp maximum at  $T_N = 2.56$  K (inset in Figure 9). Below 2.6 K, the isothermal magnetization (Fig-

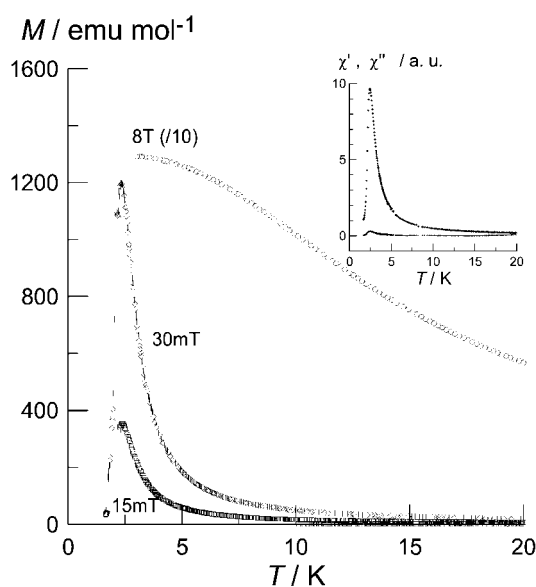


Figure 9. Magnetization temperature dependence of compound **3** under different applied magnetic fields as indicated; the inset shows the AC susceptibility,  $\chi_{AC}$ , vs.  $T$

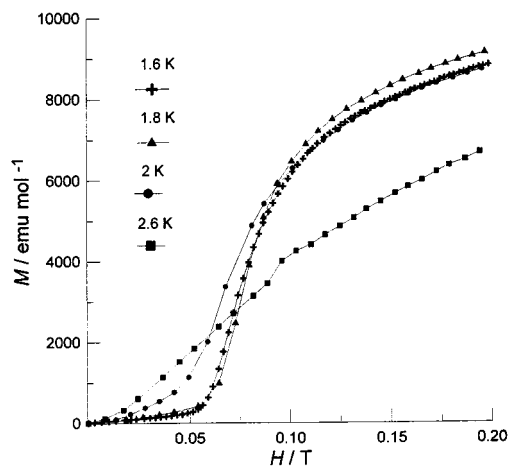


Figure 10. Magnetisation field dependence of compound **3**, at different temperatures indicated

ure 10) shows a sigmoidal field dependence, confirming the existence of a metamagnetic transition. At 1.6 K, the critical field  $H_C$ , defined as the maximum of  $dM/dH$ , is 70 mT. Above 7 T, the magnetization becomes almost saturated, attaining a value of  $2.45 \mu_B/\text{mol}$  at 12 T. This value is close to the predicted value of  $2.44 N\mu_B$ , with  $g_{Ni} = 2.07^{[1a]}$  and  $g_{Fe} = 2.81^{[1]}$ . The different measurements of DC magnetization as a function of temperature at several magnetic field strengths and of AC susceptibility as a function of field and temperature led to the tentative phase diagram shown in Figure 11.

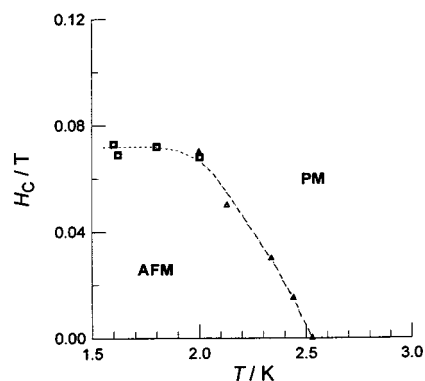


Figure 11. Critical field temperature dependence for compound **3**

Metamagnetism results from the existence of magnetic anisotropy. For compound **3**, this anisotropy can only be assigned to a different magnetic nature of the  $S \cdots C$  contacts in the  $b,c$  layers, corresponding to DA contacts from the alternating 1D DA chains, and in the  $a,b$  layers, corresponding to the AA contacts in the acceptor layers. The negative  $\theta$  value obtained for the isostructural CT salt **4** suggests that in the  $a,b$  layers the AA interactions are antiferromagnetic, which would imply that the DA interactions from the  $b,c$  layers are ferromagnetic. It is envisaged that this could be confirmed by single-crystal experiments, since if the linear chains in the  $b,c$  plane show a ferromagnetic coupling, then an antiferromagnetic behaviour should be observed along a perpendicular direction. Unfortunately,

however, it has not yet been possible to grow crystals large enough to perform such experiments.

In order to achieve a better understanding of the magnetic behaviour of the CT salt **3**, efforts will be made to obtain large single crystals. This should also allow a more detailed study of the phase diagram, which we hope to report in a subsequent publication along with the analogous salts with the donors  $[\text{Mn}(\text{Cp}^*)_2]^+$  ( $S = 1$ ) and  $[\text{Cr}(\text{Cp}^*)_2]^+$  ( $S = 3/2$ ).

## Conclusion

In conclusion, we have prepared and characterized a new nickel complex  $[\text{Ni}(\alpha\text{-tpdt})_2]^-$ , based on a thiophenedithiolate ligand that was previously described as coordinating a gold atom. The  $n\text{Bu}_4\text{N}^+$  salt of this complex shows ferromagnetic interactions, a full understanding of which will require a crystal structure determination. From this complex, decamethylmetallocenium-based CT salts have been obtained.  $[\text{Fe}(\text{Cp}^*)_2][\text{Ni}(\alpha\text{-tpdt})_2]$  displays a metamagnetic behaviour with  $T_N = 2.56$  K and a critical field of 70 mT at 1.6 K. Comparison of the magnetic properties of this compound with those of analogous salts with the diamagnetic acceptor  $[\text{Au}(\alpha\text{-tpdt})_2]^-$  and the diamagnetic donor  $[\text{Co}(\text{Cp}^*)_2]^+$  indicates that the metamagnetism is associated with the existence of ferromagnetically coupled alternating DA chains, forming layers in the  $b,c$  plane, together with antiferromagnetically acceptor-coupled layers in the perpendicular  $a,b$  plane.

The possibility of combining this complex with suitable donors to prepare conducting materials with paramagnetic anions as well as new magnetic materials is currently being explored and will be reported in due course.

## Experimental Section

**General Remarks:** All manipulations were carried out with the exclusion of air under nitrogen or argon (CV), unless stated otherwise. The starting ketone, 5,6-thieno[2,3-*d*]-1,3-dithiol-2-one, and the tetrabutylammonium salt of gold(III) bis(2,3-thiophenedithiolate),  $n\text{Bu}_4\text{N}[\text{Au}(\alpha\text{-tpdt})_2]$ , were prepared following the method used in ref.<sup>[7]</sup> All solvents were purified following standard procedures. Other chemicals were obtained commercially and were used without further purification. – Column chromatography was carried out on silica gel S (0.063–0.2 mm). – UV/vis spectra were recorded on a Cary 5G spectrophotometer (Varian). – IR spectra were recorded on a Perkin–Elmer 577 spectrophotometer. –  $^1\text{H}$  NMR: Bruker Aspect 3000 (300 MHz for  $^1\text{H}$ ),  $\text{CD}_2\text{Cl}_2$  as solvent, TMS as internal reference. – MALDI mass spectra were obtained in time-of-flight linear mode on a Kratos Kompact MALDI 2 K probe apparatus (Kratos Analytical) operated through pulsed extraction of the ions. – Cyclic voltammetry data were obtained using an EG&G PAR 263A potentiostat galvanostat on a cell equipped with a double KCl (3 M) bridge. Measurements were made at room temperature in dichloromethane and acetonitrile solutions containing  $n\text{Bu}_4\text{NPF}_6$  as the supporting electrolyte at a scan rate of 100 mV/s, using platinum wire working and counterelectrodes and an Ag/AgCl reference electrode.

**Tetrabutylammonium Salt of Nickel(III) Bis(2,3-thiophenedithiolate),  $n\text{Bu}_4\text{N}[\text{Ni}(\alpha\text{-tpdt})_2]$  (**2**):** To a stirred solution of potassium methoxide in methanol (10 mL, 2 M) was added 5,6-thieno[2,3-*d*]-1,3-dithiol-2-one (**1**) (100 mg, 0.57 mmol). The resulting yellow solution was filtered and the filtrate was added to a solution of nickel dichloride (107.7 mg, 0.29 mmol) in methanol (2 mL) yielding a red mixture. The inorganic precipitate was removed and the supernatant was added to a solution of tetrabutylammonium iodide (207.4 mg, 0.58 mmol) in methanol (1 mL). No visible change occurred while the solution was kept under an inert atmosphere. When it was stirred open to the air in an ice bath, the colour changed to green and a dark-green crystalline precipitate appeared. This solid was collected by filtration and recrystallized from acetone/2-propanol to afford dark-green, plate-like crystals. Stirring was maintained in all steps until no further modification was observed. Yield 151 mg (89%). –  $\text{C}_{24}\text{H}_{40}\text{NNiS}_6$  (593.7): calcd. C 48.56, H 6.79, N 2.36, S 32.40; found C 49.01, H 6.51, N 2.38, S 32.93. – UV/vis ( $\text{CH}_3\text{CN}$ ):  $\lambda_{\text{max}}$  = 672, 989 nm. – M.p. 130 °C (dec.). – IR (KBr):  $\tilde{\nu}$  = 380, 390 (m, Ni–S), 500 (m), 700 (m), 780 (m), 875 (m), 1140 (s), 1345 (s), 1460 (m), 3035–3085 (m, C–H arom.). – MS:  $m/z$  (%) = 243  $[\text{M}^+]$ , 350  $[\text{M}^-]$ .

**Decamethylferrocenium Salt of Nickel(III) 2,3-Thiophenedithiolate,  $[\text{Fe}(\text{Cp}^*)_2][\text{Ni}(\alpha\text{-tpdt})_2]$  (**3**):** Saturated solutions of  $n\text{Bu}_4\text{N}[\text{Ni}(\alpha\text{-tpdt})_2]$  (30.8 mg, 52  $\mu\text{mol}$ ) and  $[\text{Fe}(\text{Cp}^*)_2]\text{BF}_4$  (58.1 mg, 0.14 mmol) in acetonitrile were mixed under an inert atmosphere with stirring. Almost immediately, a dark-green crystalline precipitate appeared. This microcrystalline powder was then recrystallized from acetonitrile to afford dark-green plates. Crystals suitable for X-ray measurements were obtained by slow evaporation of the solvent from acetonitrile solutions. Yield 24 mg (69%). –  $\text{C}_{28}\text{H}_{34}\text{FeNiS}_6$  (677.5): calcd. C 49.64, H 5.06, S 28.39; found C 49.71, H 6.00, S 28.16.

**Decamethylferrocenium Salt of Gold(III) 2,3-Thiophenedithiolate,  $[\text{Fe}(\text{Cp}^*)_2][\text{Au}(\alpha\text{-tpdt})_2]$  (**4**):** This compound was obtained according to the same method as used to prepare **3**, using  $n\text{Bu}_4\text{N}[\text{Au}(\alpha\text{-tpdt})_2]$  instead of  $n\text{Bu}_4\text{N}[\text{Ni}(\alpha\text{-tpdt})_2]$ . Yellow-gold needle-shaped crystals were obtained in 76% yield. –  $\text{C}_{28}\text{H}_{34}\text{AuFeS}_6$  (815.8): calcd. C 41.23, H 4.20, S 23.58; found C 40.72, H 4.28, S 23.51.

**Decamethylcobaltocenium Salt of Nickel(III) 2,3-Thiophenedithiolate,  $[\text{Co}(\text{Cp}^*)_2][\text{Ni}(\alpha\text{-tpdt})_2]$  (**5**):** This compound was obtained according to the same method as used to prepare **3**, using  $[\text{Co}(\text{Cp}^*)_2]\text{PF}_6$  instead of  $[\text{Fe}(\text{Cp}^*)_2]\text{BF}_4$ . Dark-green, plate-like crystals were obtained in 34% yield. –  $\text{C}_{28}\text{H}_{34}\text{CoNiS}_6$  (680.6): calcd. C 49.42, H 5.04, S 28.26; found C 49.03, H 5.13, S 27.91.

**EPR Spectroscopy:** EPR spectra in the range 4–300 K were obtained with an X-band Bruker ESP 300E spectrometer equipped with an ER041XK microwave bridge, a rectangular cavity operating in T102 mode, a Bruker variable-temperature unit, an Oxford Instruments ESR-900 cryostat, and an ER 032M field controller system. The modulation amplitude was kept well below the line width and the microwave power well below saturation.

**Magnetic Susceptibility:** Magnetic measurements were performed using either a longitudinal Faraday system (Oxford Instruments) with a 7 T superconducting magnet for static susceptibility measurements in the range 2–300 K, or a Maglab 2000 system (Oxford Instruments) for DC magnetization and AC susceptibility at fields of up to 12 T at temperatures down to 1.5 K. The Faraday system was used with a magnetic field of 2 T and forward and reverse field gradients of 5 T/m. A polycrystalline sample (10–15 mg) was placed inside a previously calibrated thin-walled Teflon® bucket. The force was measured with a microbalance (Sartorius S3D-V). The Maglab 2000 system was used for magnetization measurements

of similar polycrystalline samples at different magnetic fields using an extraction technique, and for AC susceptibility measurements using an AC field of 1 Oersted.

**X-ray Crystallographic Study:** The crystal structure was solved by direct methods.<sup>[12]</sup> Non-hydrogen atoms were refined anisotropically. Hydrogen atoms were placed in calculated positions and refined as riding on their parent carbon atoms. Further details of the crystal structure determination are given in Table 2. Graphical representations were generated using ORTEP III<sup>[13]</sup> (Figure 4) and SCHAKAL-97<sup>[14]</sup> (Figure 5–Figure 7). Experimental details such as atomic coordinates, bond lengths, and angles are available as Supporting Information. Crystallographic data (excluding structure factors) for the structure of Fe(Cp\*)<sub>2</sub>[Ni( $\alpha$ -tpdt)<sub>2</sub>] reported in this paper have been deposited with the Cambridge Crystallographic Data Centre under the depository number CCDC-152949. Copies of the data can be obtained free of charge upon application to CCDC, 12 Union Road, Cambridge CB2 1EZ, U.K. [Fax: (internat.) + 44-(0)1223/336033; E-mail: deposit@ccdc.cam.ac.uk].

Table 2. Crystallographic data for [Fe(Cp\*)<sub>2</sub>][Ni( $\alpha$ -tpdt)<sub>2</sub>] (3)

Cmpd.	Fe(Cp*) <sub>2</sub> [Ni( $\alpha$ -tpdt) <sub>2</sub> ]
Crystal system	Monoclinic
Crystal colour/Shape	Dark-green plates
Space group	<i>P2<sub>1</sub>/a</i>
Lattice constants [ $\text{\AA}$ , °]	<i>a</i> = 15.443(3) <i>b</i> = 10.237(1) <i>c</i> = 20.360(2) $\beta$ = 107.54(1)
Volume [ $\text{\AA}^3$ ]	3069.1(7)
Z	4
Empirical formula	C <sub>28</sub> H <sub>34</sub> FeNiS <sub>6</sub>
Molecular mass	677.47
Density (calcd.) [Mg/m <sup>3</sup> ]	1.466
Absorption coefficient [mm <sup>-1</sup> ]	1.511
<i>F</i> (000)	1408
Diffractometer	Enraf–Nonius CAD4
Wavelength	Mo-K $\alpha$ (0.71069 $\text{\AA}$ )
<i>T</i> [K]	293(2)
$\theta$ range[°]	2.10 to 27.04
Index range ( <i>h</i> , <i>k</i> , <i>l</i> )	–19/1, –1/13, –25/26
Scan type	$\omega$ –2 $\theta$
Program for data collection	CAD4 software
Data reduction	Process-MOLEN
No. of collected reflns.	8208
No. of independent reflns.	6640
Max. and min. transmission	0.9996/0.9172
Structure solution	Direct methods
Structure refinement	Full-matrix least-squares
Programs used	SHELXS-86 SHELXL-97
Goodness-of-fit on <i>F</i> <sup>2</sup>	1.026
No of refined parameters	328
<i>R</i> [ <i>I</i> > 2 $\sigma$ ( <i>I</i> )]	0.0976
<i>wR</i> <sub>2</sub> [ <i>I</i> > 2 $\sigma$ ( <i>I</i> )]	0.1215

## Acknowledgments

This work was partially supported by the Fundação para a Ciência e Tecnologia (Portugal) under contracts PRAXIS XXI 2/2.1/QUI/203/94 and POCTI/1999/QUI/35452 and by the Comisión Interministerial de Ciencia y Tecnología (MAT2000-1388-C03-01) and the Generalitat de Catalunya (2000SGR-00114) (Spain). The collaboration between the team members of Sacavém and Barcelona was supported under the CSIC-ICCTI bilateral agreement and by COST action D14.

- [1] [1a] J. A. McCleverty, *Prog. Inorg. Chem.* **1968**, *10*, 29. – [1b] D. Coucouvanis, *Prog. Inorg. Chem.* **1970**, *11*, 233. – [1c] R. Eisenberg, *Prog. Inorg. Chem.* **1970**, *12*, 295. – [1d] L. Alcácer, H. Novais, in: *Extended Linear Chain Compounds*, Vol. 3 (Ed.: J. S. Miller), Plenum Press, New York, **1983**, chapter 6, p. 319. – [1e] S. Alvarez, R. Vicente, R. Hoffman, *J. Am. Chem. Soc.* **1985**, *107*, 6253–6277.
- [2] [2a] A. E. Underhill, M. Ahamad, *J. Chem. Soc., Chem. Commun.* **1981**, 67–68. – [2b] M. M. Ahamad, D. J. Turner, A. E. Underhill, C. S. Jacobsen, K. Mortensen, K. Carneiro, *Phys. Rev. B* **1984**, *29*, 4796.
- [3] P. Cassoux, L. Valade, in: *Inorganic Materials*, 2nd edn. (Eds.: D. W. Bruce, D. O'Hare), John Wiley and Sons, Chichester, **1996**, p. 1–64.
- [4] P. Cassoux, J. S. Miller, in: *Chemistry of Advanced Materials* (Eds.: L. V. Interrante, M. J. Hampden-Smith) Wiley-VCH, New York, **1998**, p. 19–72.
- [5] I. D. Parker, R. H. Friend, P. I. Clemenson, A. E. Underhill, *Nature (London)* **1986**, *324*, 547–548.
- [6] [6a] V. Gama, D. Belo, S. Rabaça, I. C. Santos, H. Alves, M. T. Duarte, J. C. Warenborg, R. T. Henriques, *Eur. J. Inorg. Chem.* **2000**, *9*, 2101–2110; W. E. Broderick, J. A. Thompson, B. M. Hoffman, *Inorg. Chem.* **1991**, *30*, 2958–2960. – [6b] V. Gama, S. Rabaça, C. Ramos, D. Belo, I. C. Santos, M. T. Duarte, *Mol. Cryst. Liq. Cryst.* **1999**, *335*, 81–90.
- [7] D. Belo, H. Alves, E. B. Lopes, M. T. Duarte, V. Gama, R. T. Henriques, M. Almeida, A. Pérez-Benítez, C. Rovira, J. Veciana, *Chem. Eur. J.* **2001**, *7*, 511–519.
- [8] W. E. Broderick, J. A. Thompson, M. R. Godfrey, M. Sabat, B. M. Hoffman, *J. Am. Chem. Soc.* **1989**, *111*, 7656–7659.
- [9] C. Mahadevan, M. Seshasayer, P. Kuppusamy, P. T. Manoharan, *J. Cryst. Spectrosc. Res.* **1985**, *15*, 305–316.
- [10] E. Ribera, C. Rovira, J. Veciana, J. Tarrés, E. Canadell, R. Rousseau, E. Molins, M. Mas, J.-P. Schoeffel, J.-P. Pouget, J. Morgado, R. T. Henriques, M. Almeida, *Chem. Eur. J.* **1999**, *5*, 2025–2039.
- [11] J. S. Miller, J. C. Calabrese, H. Rommelmann, S. R. Chittipeddi, J. H. Zhang, W. M. Reiff, A. J. Epstein, *J. Am. Chem. Soc.* **1987**, *109*, 769–781.
- [12] [12a] G. M. Sheldrick, *Acta Crystallogr., Sect. A* **1990**, *46*, 467. – [12b] G. M. Sheldrick, *SHELXL-93 – Program for the Refinement of the Crystal Structures*, University of Göttingen, Germany, **1993**. – [12c] G. M. Sheldrick, *SHELXL-97 – Program for the Refinement of the Crystal Structures*, University of Göttingen, Germany, **1997**, release 97–2.
- [13] P. McArdle, *J. Appl. Cryst.* **1995**, *28*, 65.
- [14] E. Keller, *SCHAKAL-97 – A Computer Program for the Graphical Representation of Molecular and Crystallographic Models*, Kristallographisches Institut der Universität Freiburg, Hebelstrasse 25, D-79104 Freiburg, Germany.

Received July 5, 2001  
[I01251]